JOURNAL OF GEOPHYSICAL RESEARCH, VOL. 95, NO. C6, PAGES 9679–9688, JUNE 15, 1990

Measurements of Sea Spikes in Microwave Backscatter at Moderate Incidence

A. T. JESSUP

Ralph M. Parsons Laboratory, Massachusetts Institute of Technology, Cambridge

W. C. KELLER

U.S. Naval Research Laboratory, Washington, D. C.

W. K. MELVILLE

Ralph M. Parsons Laboratory, Massachusetts Institute of Technology, Cambridge

Previous authors have associated large events, or "sea spikes", in the radar cross section of the sea surface with steep or breaking waves. Here we present a method based on an intensity threshold and the mean Doppler frequency to identify and quantify sea spikes likely to be associated with large-scale wave breaking. This method is applied to microwave measurements of K_u band made with a dual-polarized Doppler scatterometer at a moderate incidence angle (45°) from a fixed platform in the North Sea. For *VV* and *HH* polarization the mean normalized radar cross section σ^0, the frequency of sea spike occurrence *N*, and the sea spike contribution to the mean normalized radar cross section, σ^0_{SS}, are correlated with direct measurements of the friction velocity, u_*, in the range $13 \le u_* \le 49$ cm s^{-1}. The friction velocity exponents for both *N* and σ^0_{SS} indicate an approximately cubic dependence, while the residual radar cross section $\sigma^0_{\mathrm{res}} = \sigma^0 - \sigma_{SS}$ is approximately proportional to friction velocity for u_* greater than approximately 20 cm s^{-1}. At high friction velocities, ($u^* \approx 40$–50 cm s^{-1}) these data show that the contribution of large sea spikes to the mean radar cross section for measurements between 25° and 45° relative to the wind is in the range of 5–10% for *VV* polarization and 10–20% for *HH* polarization.

1. INTRODUCTION

Spiky fluctuations in radar return at grazing incidence angles have long been associated with steep and breaking waves [*Katzin*, 1957; *Long*, 1974, 1983; *Kalmykov and Pustovoytenko*, 1976] and have been generally referred to as "sea spikes." Simultaneous video recordings were used by *Lewis and Olin* [1980] to show that high-amplitude sea spikes correspond to the development and decay of whitecaps, while *Ewell et al.* [1984] tracked sea spikes that moved with a speed approximately equal to the phase speed of the dominant ocean waves.

Sea spikes are also evident in moderate incidence angle measurements and have been attributed to various mechanisms associated with the steep crests of breaking waves [*Alpers et al.*, 1981]. *Keller et al.* [1986] presented field observations which correlated Doppler spectra with breaking events, indicating that the scatterer speed during breaking increased toward the phase speed of the dominant waves and that the Doppler bandwidth was greatly increased. They suggested that the scattering may include contributions from specular surface reflections and that a coherent microwave radar may be the ideal instrument for quantitative study of wave breaking. A limited set of video recordings made simultaneously with moderate incidence angle scatterometer measurements have shown that sea spikes are consistently associated with visual evidence of wave breaking [*Jessup*, 1988].

Paper number 89JC03347.
0148-0227/90/89JC-03347$05.00

Duncan et al. [1974] observed scattering at moderate incidence angles due to wave breaking in the laboratory which was independent of polarization and was a major contributor to the return at high wind speeds. *Kwoh and Lake* [1984, 1986] measured the relative contributions to *X* band microwave return from mechanically generated water waves due to specular and nonspecular reflections. The specular contribution was attributed to either the turbulent wake of breaking or the steep capillary waves generated in the process, while the nonspecular return was attributed to wedgelike diffraction from the small radius crests of breaking or near-breaking waves. More recently, *Kwoh et al.* [1988] presented field measurements supporting the association of specular return with wave breaking. *Banner and Fooks* [1985] made *X* band microwave measurements of stationary small-scale breaking waves generated in a flume and found that high levels of backscattered power were associated with the breaking region. They concluded that the measured backscatter was consistent with Bragg scattering from hydrodynamic disturbances generated just ahead of the breaking crest. A number of the proposed scattering mechanisms associated with sharp-crested and breaking waves have been used to improve predictions based on the composite model, especially for horizontal polarization [*Lyzenga et al.*, 1983; *Donelan and Pierson*, 1987].

Phillips [1988] has recently considered the friction velocity dependence of the frequency of occurrence of sea spikes and their contribution to the radar cross section. He proposes that for moderate incidence angles the mean normalized radar cross section σ^0 is the sum of separate contributions from Bragg scattering σ_B^0 and from sea spikes σ_{SS}^0 associated with localized breaking events:

$$\sigma^0 = \sigma_B^0 + \sigma_{SS}^0 \tag{1}$$

The small perturbation model for backscattering from the sea surface [*Wright*, 1966] was combined with an expression for the ocean gravity wave spectral density $\psi(\mathbf{k})$ under equilibrium conditions [*Phillips*, 1985]:

$$\psi(\mathbf{k}) = \beta|\cos\varphi|^{1/2} u_* g^{-1/2} k^{-7/2} \tag{2}$$

where β is a constant, k is the ocean wave number, φ is the angle between the wind and wave propagation direction, and g is the gravitational acceleration. The Bragg contribution σ_B^0 was then given by

$$\sigma_B^0 = \frac{\pi\beta}{2\sqrt{2}} |\cos\varphi|^{1/2} \sin^{1/2}\theta \cot^4\theta \, F_1(\theta)(u_*^2\kappa/g)^{1/2} \tag{3}$$

where θ is the incidence angle and κ is the electromagnetic wave number. The function $F_1(\theta)$ in general will depend on the transmitted and received polarization as well as θ. The form of $\psi(\mathbf{k})$ given by (2) is valid for wave numbers in the gravity wave range whose phase speed is large compared with u_*. Thus k must satisfy the condition

$$k_0 \ll k < \min\{(g/\gamma)^{1/2}, g/u_*^2\} \tag{4}$$

where k_0 is the wave number of the peak of the wave spectral density and γ is the surface tension of water divided by its density. This condition and the Bragg condition,

$$k = 2\kappa \sin\theta \tag{5}$$

lead to the following constraint on the electromagnetic wave number:

$$2\kappa \sin\theta < \min\{(g/\gamma)^{1/2}, g/u_*^2\} \tag{6}$$

Equation (3) predicts that the contribution from Bragg scattering varies linearly with friction velocity u_* for a given radar frequency, incidence angle, and azimuth angle φ. Measurements of radar backscatter in the frequency range 0.4 to 9 GHz from *Guinard et al.* [1971] were used by Phillips to support the frequency and friction velocity dependence of (3). Strictly speaking, the form of the wave spectral density (equation (2)) is valid only in the gravity wave range. Thus the comparison of (3) with radar measurements in the centimeter range of wavelengths may be questioned.

On the basis of previous work concerning the energy dissipation due to wave breaking [*Phillips*, 1985], Phillips derived an expression for σ_{SS}^0, the contribution of sea spikes to the mean normalized radar cross section:

$$\sigma_{SS}^0 \approx F_2(\theta, \chi)[u_*^2\kappa/g]^{3/2} \tag{7}$$

where χ is the angle between the radar look direction and the wind. Equation (7) predicts that for a given measurement geometry and radar frequency, the contribution of sea spikes to σ^0 is proportional to the friction velocity cubed.

Finally, a cubic dependence on friction velocity was found for the frequency of sea spike occurrence per unit area,

$$\nu(k_1) \propto g^{-1} k_1^4 u_*^3 \tag{8}$$

where k_1 is a threshold wave number significantly larger than that of the spectral peak. Phillips asserts that breaking events associated with large wavelengths may be expected to produce more intense returns and that setting a radar cross section threshold of intensity above which a sea spike is counted corresponds to identifying breaking events associated with wave numbers below the threshold wave number k_1. If sea spikes are caused by scattering from whitecaps, then (8) is consistent with theoretical modeling which indicates that the whitecap coverage should vary as u_*^3 [*Wu*, 1979] and with correspondingly large wind speed exponents for various measurements of whitecap coverage [*Ross and Cardone*, 1974; *Wu*, 1980; *Monahan and O'Muircheartaigh*, 1986].

Most recently, *Melville et al.* [1988] have reported measurements of microwave scattering and sound generation by controlled breaking events in the laboratory. They found that the dissipation due to breaking correlated almost linearly with both the backscattered microwave power and the radiated acoustic power. If these results carry over to the field, microwave observations of breaking may yield important dynamic and acoustic information on the wave field and the upper ocean.

In order to investigate the statistics of sea spikes and their contribution to the mean normalized radar cross section, measurements of microwave backscatter, friction velocity, and wave height made during a 2-week period in May 1987 from the German research platform NORDSEE were analyzed. The platform is located in 30 m of water approximately 40 n. mi (76 km) off the German peninsula in the North Sea [see *Keller et al.*, 1989]. These measurements were performed in conjunction with the installation of a system for studying the long-term variation of the mean radar cross section; thus the experiment was not specifically designed to study the sea spikes associated with wave breaking, and the data set is of limited duration. Nevertheless, these measurements provide the first quantitative analysis of sea spikes over a range of environmental conditions by presenting the friction velocity dependence of their frequency of occurrence and their contribution to the mean normalized radar cross section. A more detailed account of these results and subsequent related measurements from the SAXON-CLT experiment is given by *Jessup* [1990].

2. Experimental Procedure and Data Analysis

The microwave backscatter measurements were made using a coherent, continuous-wave, dual-polarized scatterometer operating at 14 GHz (K_u band, wavelength of 2.14 cm) with a transmit power of 200 mW. The instrument was designed, built, and calibrated at the U.S. Naval Research Laboratory, Washington, D. C. The instrument incorporates linear dual-polarized antennas which allow simultaneous vertical (VV) and horizontal (HH) like-polarization measurements. In-phase and quadrature channels at base band for both polarizations provide a complex time series output. The envelope of the signal is proportional to the received power, and its rate of change of phase is the Doppler shift frequency. The complex output scheme permits discrimination of positive and negative target velocities. The instrument was mounted 31 m above the mean sea surface, aimed with an incidence angle of 45° and pointed northwest at 315°T. In this configuration the measurement was well within the far field of the antennas, and the two-way 3-dB elliptical illumination area on the sea surface was approximately 1.8 × 2.5 m^2. The radar was calibrated with a swinging sphere, and the absolute normalized radar cross-section values quoted here are accurate to within ±1 dB. The sea spike results are dependent not on the accuracy of the measurement but

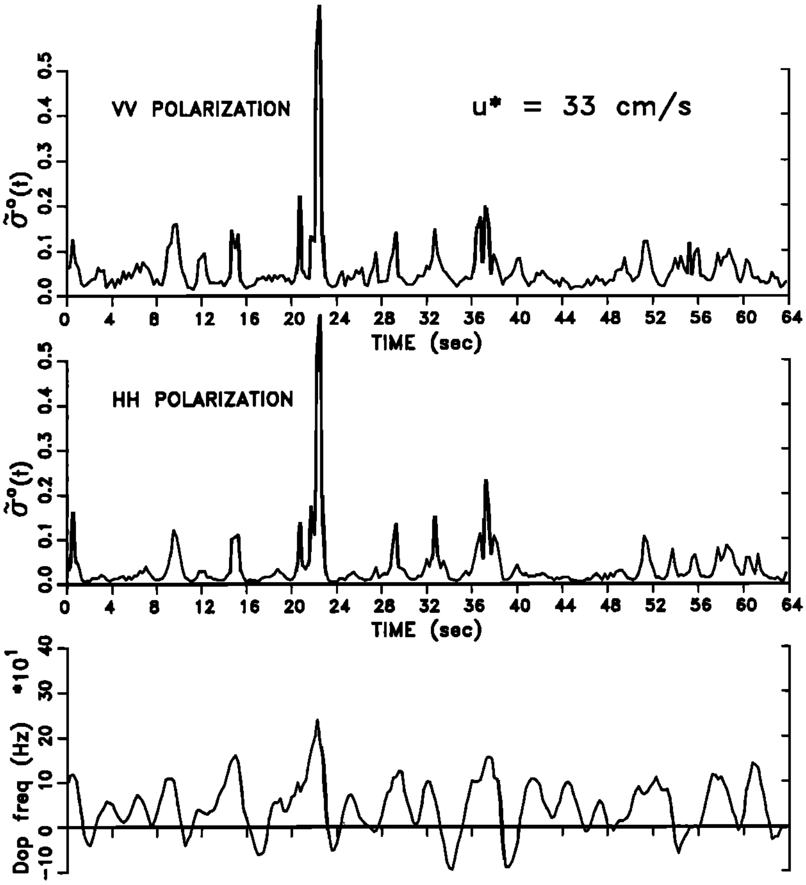

Fig. 1. Simultaneous time series (64 s) of the normalized radar cross section $\tilde{\sigma}^0(t)$ for *VV* and *HH* polarization and mean Doppler frequency for *VV*. The sea spike at approximately 23 s, with a large jump in $\tilde{\sigma}^0(t)$ coincident with a Doppler frequency maximum is typical of those associated with breaking events.

rather on its precision, or the relative stability of the calibration over time. Experience with systems of similar design indicates that the relative measurement error is less than ±0.5 dB.

Direct measurements of friction velocity were provided by Risø National Laboratory, Roskilde, Denmark, using a sonic anemometer (Kaijo-Denki, model DAT-300 with probe head type TR-61-B) mounted on a boom extending 20 m due west of the platform at a height of 33 m above the sea surface. Wave height measurements from the Baylor gauge permanently installed on the platform were used to obtain a characteristic phase speed with which to normalize the Doppler velocity measurements.

The radar output and wave height data were recorded on a Hewlett-Packard HP3968A FM analog tape recorder (bandwidth of 625 Hz), while the data acquisition system for the sonic anemometer produced 10-min averages of the friction velocity u_* in real time. The microwave signal was digitally sampled at 2 kHz and reduced to time series of the received power and the mean Doppler frequency with an averaging time of 0.25 s. The mean Doppler frequency was computed using an autocovariance estimation technique commonly used for Doppler weather radar [*Doviak and Zrnić*, 1984]. Comparison of this technique with calculation of the first moment of the Doppler spectrum using Fourier transform methods showed excellent agreement.

The normalized radar cross section is proportional to the backscattered power averaged over the illumination area; the notation σ^0 often implies an additional time average. In an effort to avoid confusion, we will use σ^0 to denote the time-averaged normalized radar cross-section and $\tilde{\sigma}^0(t)$ to be the time series from which σ^0 is computed, that is,

$$\sigma^0 = \frac{1}{T}\int_0^T \tilde{\sigma}^0(t)\, dt \tag{9}$$

for a time series of length T.

In a typical open ocean environment, 10–15% or fewer of the wave crests passing a fixed location might be breaking [*Holthuijsen and Herbers*, 1986]. Thus a relatively long time record must be used in order to provide enough samples to ensure the statistical significance of an analysis based on counting events. On the other hand, the time record should not be so long that the environmental conditions have drastically changed. For our analysis a record length of 1-hour was chosen over which to compute the averages of interest. Out of a total of approximately 80 hours of analog tape recordings, 48 hours of data have been selected for this analysis.

Figure 1 is an example of a 64-s time series of processed data which includes a typical sea spike. The two top traces show the variation of $\tilde{\sigma}^0(t)$ on a linear scale for *VV* and *HH* polarization. The mean Doppler frequency shown in the bottom trace is proportional to the line-of-sight component of the surface scatter velocity averaged over the illumination area, which is dominated by the orbital velocity of the long surface waves [*Plant and Keller*, 1983]. For both polarizations the sea spike at approximately 23 s is characterized by

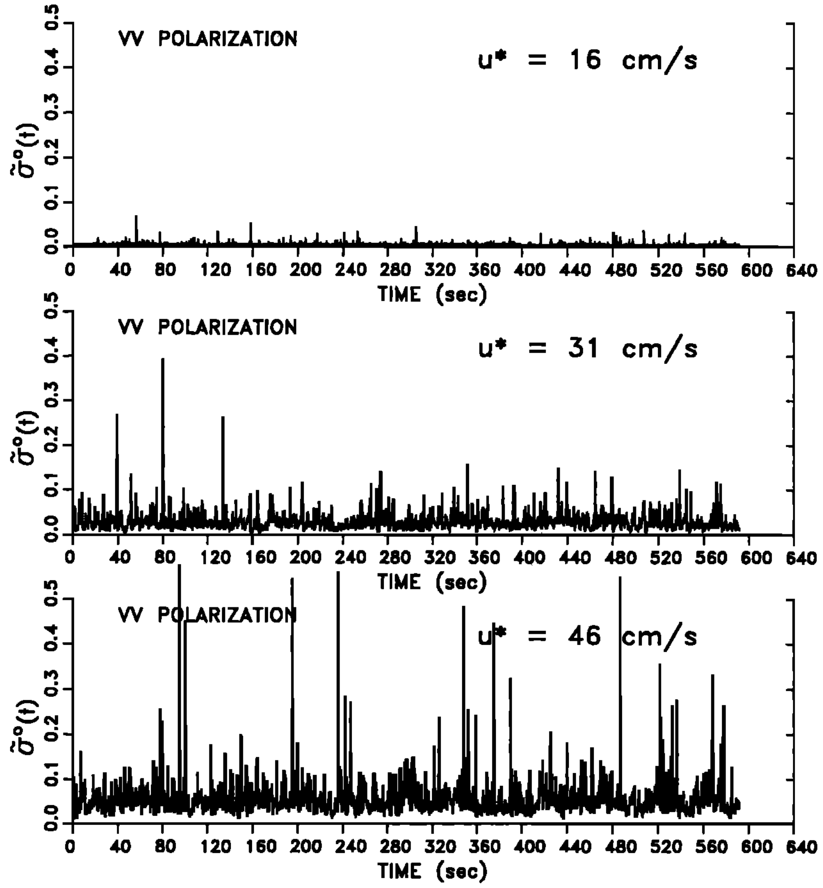

Fig. 2. Comparison of time series (10 min) of radar cross-section, $\tilde{\sigma}^0(t)$, for *VV* polarization showing the qualitative difference in frequency of occurrence of sea spikes with increasing friction velocity u_*.

a large excursion in backscattered power and a local maximum in the Doppler frequency.

Comparison of the time series of radar cross section for increasing values of friction velocity illustrates qualitatively how the frequency of occurrence of sea spikes increases. Figure 2 shows three representative time series of length 10 min of *VV* radar cross-section data for different values of u_*. The top trace is for a low value of 16 cm s^{-1}, for which little or no breaking would be expected. In addition to an increase in the mean radar cross section, the number of sea spikes is increased in the second and third traces, for which the friction velocity is 33 cm s^{-1} and 46 cm s^{-1}, respectively.

Wave breaking is a process that occurs over a wide range of scales, from small-scale or microscale breaking [*Phillips and Banner*, 1974] through intermediate-sized breaking events, which may not produce discernible foam patches, to larger events that generate whitecaps. Figures 1 and 2 illustrate that the amplitudes of spikes in σ^0 also occur over a wide range of scales. As was noted already, previous authors have associated large sea spikes with breaking waves, that is, events that produce whitecaps. The correlation of lesser-amplitude spikes with smaller-scale breaking is unclear without supplementary information such as a video image. We also note that Phillips' expression for the frequency of sea spike occurrence (equation (8)), was derived for "larger-scale breakers producing the more intense return" [*Phillips*, 1988, p. 1070]. To avoid the ambiguity associated with smaller sea spikes and for comparison with (8), we will concentrate on detecting sea spikes that are likely to be associated with larger-scale breaking events. Furthermore, we will take larger-scale breaking events to be those occurring at or near the long wave crests. Thus our detection scheme should identify large sea spikes associated with the long wave crests.

From comparison of the time series of the radar cross section and the mean Doppler shift (see Figure 1), large spikes in the return power are clearly associated with large positive surface velocities, corresponding to measurements at or near the long wave crests. Scatter plots of the distribution of the measured velocity for *VV* polarization as a function of the peak value of $\tilde{\sigma}^0(t)$ for two different friction velocities are shown in Figure 3. The Doppler frequency is proportional to the areal average of the line-of-sight component of the surface scatterer velocities, which we assume to be nearly horizontal at a wave crest. The measured velocity values in Figure 3 have been resolved to be horizontal, which is appropriate for the larger sea spikes associated with large velocities (the lower velocity values associated with parts of the wave other than the crest are corrupted). Since the crest velocity of a breaking wave is expected to be of the order of its phase speed, the measured velocities have been normalized by the phase speed corresponding to the wave spectral density peak.

Figure 3*a* is for a friction velocity of 28 cm s^{-1}, while Figure 3*b* is for a higher value of 49 cm s^{-1}. In both cases, low values of $\tilde{\sigma}^0_{\mathrm{peak}}$ correspond to negative velocities, which indicate return from a location away from a wave crest. Above some threshold, only positive velocities are found, and the more intense returns are associated with larger positive velocities. Scatter plots for each hour of data

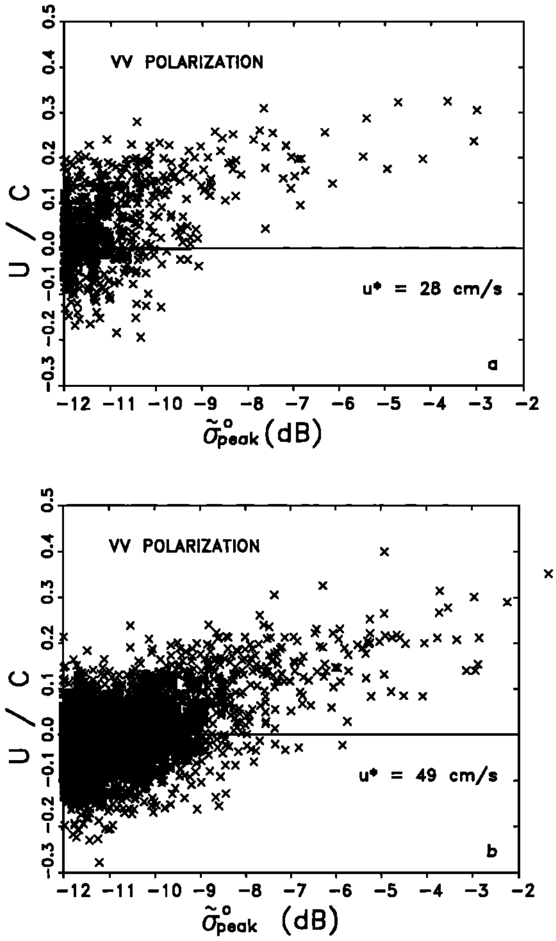

Fig. 3. Scatter plots showing the distribution of normalized surface scatterer velocity for peak radar cross section (VV) for two different friction velocities: (a) $u_* = 28$ cm s^{-1} and (b) $u_* = 49$ cm s^{-1}. The detection threshold of -7.2 dB has been chosen to detect mainly sea spikes associated with a positive velocity, corresponding to a location near a long wave crest.

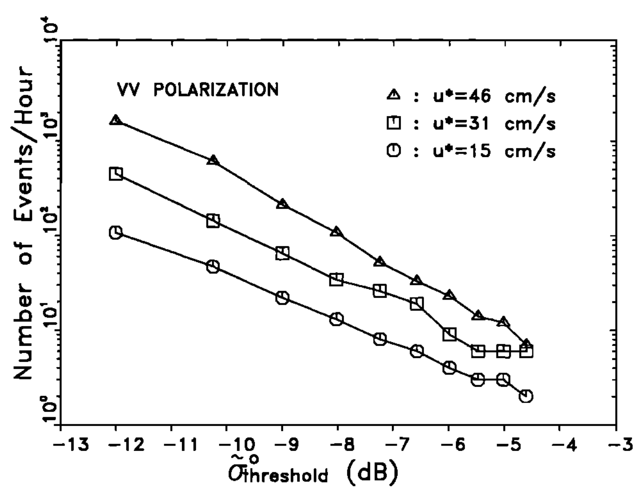

Fig. 4. The number of sea spikes, N, in a 1-hour record as a function of radar cross-section detection threshold over a wide range of friction velocities, u_*. The relatively constant slope and spacing of curves indicates that sea spike statistics are not strongly dependent on threshold over a range of several decibels.

processed have been analyzed, and a threshold of $\tilde{\sigma}^0(t) = -7.2$ dB has been chosen to eliminate most large sea spikes associated with negative velocities for both VV and HH polarizations over a friction velocity range of $15 \leq u_* \leq 49$ cm s^{-1}.

The use of a fixed threshold for analyzing data over a wide range of friction velocity may at first seem inappropriate, since from Figure 3 the $\tilde{\sigma}^0_{\text{peak}}$ values at which negative velocities are eliminated appears to be a function of u_*. However, consider the implication of Phillips' assertion (noted in section 1) that sea spike intensity should increase with the wavelength or scale associated with the breaking event. If we accept this assertion and assume that the sea spike intensity corresponding to a particular scale of breaker is not itself a function of u_*, then a fixed detection threshold is appropriate for detecting events in the same range of scale regardless of u_*.

The usefulness of a counting technique would be enhanced if the sea spike properties were relatively insensitive to the choice of detection threshold over some reasonable intensity range. In order to investigate this threshold dependence, we have counted the number of sea spikes in 1-hour records as a function of the cross-section threshold for different friction velocities. Examples of this analysis for three different velocities are given in Figure 4, showing that for a given u_* the number of events decreases as the threshold increases. The relatively constant slope and spacing of these curves over a threshold range of several decibels indicates that the sea spike statistics may not be especially sensitive to the choice of threshold. That is, the relative change between curves of different u_* for a given threshold is not a strong function of that threshold. To quantify the threshold dependence of the sea spike statistics presented below, the detection threshold was varied over a range of approximately 3 dB, centered at the chosen level of -7.2 dB.

The threshold of -7.2 dB is supported by previous analysis of video recordings taken during the experiment [*Jessup*, 1988]. One hour of simultaneous radar and video measurements ($u_* = 26$ cm s^{-1}) were made by visually aligning the radar antennas and video camera to be aimed at approximately the same location on the sea surface. A spectrum analyzer connected to one channel of the radar output was then used in conjunction with a video monitor to optimize the alignment. Although there was no way to measure the accuracy of the alignment, the presence of a whitecap on the video monitor was repeatedly associated with a large jump in received power and increased Doppler frequency. Unfortunately, the quality of the video recording was seriously degraded by a mismatch in video formats between the camera and recording unit.

Despite the alignment uncertainty and the poor recording quality, the 1-hour video tape was carefully reviewed in conjunction with the simultaneous microwave measurements to yield useful but limited quantitative information. The radar data were played into a spectrum analyzer to produce time histories of Doppler spectra in a waterfall or spectral map display. A total of 82 events that exhibited a microwave signature characteristic of breaking events were identified from the Doppler maps. The video tape was independently viewed and a total of 71 whitecaps were counted. Because of the poor quality of the video, no attempt was made to classify the size or scale of the whitecaps identified.

Although the number of events counted independently in the radar and video recordings were roughly the same, only 43 breaking events were simultaneously found in both the radar and video recordings. Nonetheless, approximately 70% of the events which simultaneously appeared as whitecaps on the video monitor and were identified in the Doppler spectral maps were subsequently detected by the intensity threshold of −7.2 dB. The discrepancy between the number of independently counted and simultaneously occurring events may be due to (1) misalignment of the radar and video spots, (2) the radar's detecting breaking events that do not produce a whitecap, and (3) whitecap events that do not produce a distinctive microwave signature. A breaking event which does not produce a noticeable whitecap may correspond to the intermediate scale breaking mentioned previously, while a whitecap whose propagation direction is oblique to the radar look direction may not produce a distinctive microwave signature. The uncertainty in alignment of the radar and video spots and the poor quality of the video recording have frustrated attempts to extract further meaningful results from these simultaneous measurements.

By analogy with the computational definition of σ^0 given by (9), the mean normalized sea spike radar cross section σ^0_{SS} corresponding to the sea spike contribution to σ^0 is

$$\sigma^0_{SS} = \frac{1}{T} \sum_{i=1}^{N} \int_{T_i} \tilde{\sigma}^0_{SS}(t)\, dt \tag{10}$$

where $\tilde{\sigma}^0_{SS}(t)$ is the contribution of an individual sea spike, N is the number of sea spikes in a record of length T, and T_i is the duration of the ith event.

The two methods we have chosen to define an individual sea spike intensity and duration are illustrated in Figure 5. For method 1, T_i is the time over which the radar cross section is elevated above the mean, σ^0, and $\tilde{\sigma}^0_{SS}(t)$ is that portion of the total cross-section which is above the mean during T_i:

$$\tilde{\sigma}^0_{SS}(t) = \tilde{\sigma}^0(t) - \sigma^0 \tag{11}$$

The duration T_i for method 2 is the time between local minima on either side of the sea spike maximum, and $\tilde{\sigma}^0_{SS}(t)$ is given by

$$\tilde{\sigma}^0_{SS}(t) = \tilde{\sigma}^0(t) - \tilde{\sigma}^0_{\min} \tag{12}$$

where $\tilde{\sigma}^0_{\min}$ is the lesser of the local minima defining T_i. While other methods are possible, these two provide reasonable upper and lower bounds on the contribution of an individual sea spike.

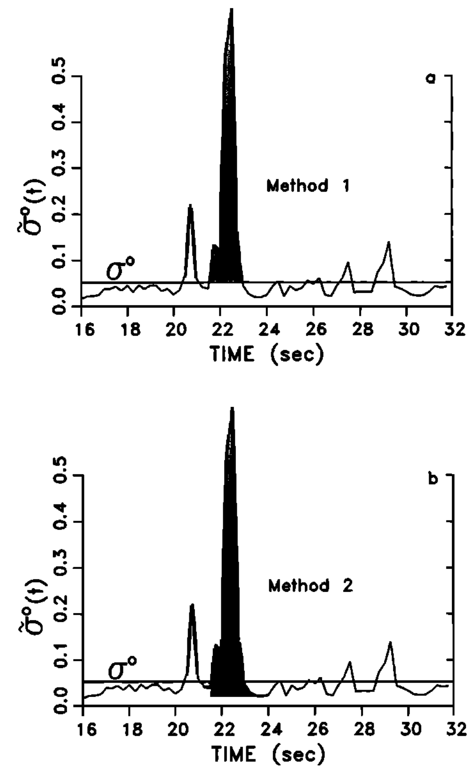

Fig. 5. A schematic diagram showing the two methods used to compute the sea spike contribution to the normalized radar cross-section. The horizontal line labeled σ^0 is the normalized radar cross-section for a one-hour record. The contribution of an individual sea spike corresponds to the shaded area. The duration of the sea spike in method 1 (Figure 5*a*) is taken as the time during which $\tilde{\sigma}(t)$ is elevated above the mean σ^0. In method 2 (Figure 5*b*) the spike duration is taken as the time between local minima on either side of the sea spike peak.

3. RESULTS

The measured mean normalized radar cross section σ^0 is plotted versus friction velocity u_* on a log-log scale for *VV* and *HH* polarization in Figure 6, where each point represents the mean for a 1-hour record. The radar antennas remained fixed during the experiment, pointing in the NW direction of 315°T. All data analyzed were for wind directions in the angular bands 340°–360° or 270°–280°. That is, the angle φ between the radar look direction and the wind was between 25° and 45° for all measurements. These data are presented together, since the variation of σ^0 is expected to be symmetric about $\varphi = 0$ and the range of φ variation for the data is 20° or less. The data at higher friction velocities in Figure 6 appear to be highly correlated, but the scatter at lower values of u_* suggests that a linear fit over the entire range of u_* is not appropriate.

The cross section of an individual breaking event is expected to be a function of the orientation of its crest with respect to the radar look direction. A reasonable assumption is that the directional distribution of breaking wave crests is symmetric about the wind. Then upwind measurements made over a restricted range of the angle φ between the radar look direction and the wind should provide a valid sampling of breaking events, even if that angular range is not centered at $\varphi = 0$.

The sea spike contribution σ^0_{SS} as defined by method 1 (equations (10) and (11) and Figure 5*a*) is shown versus friction velocity u_* on a log-log plot in Figure 7 for the cross-section threshold of −7.2 dB. For the relation

$$\sigma^0_{SS} = C_1 u_*^{\alpha} \tag{13}$$

we find the exponent α of the least squares linear fit to be 3.3 and 3.5 for *VV* and *HH* polarizations, respectively. The exponent α does not vary greatly over a threshold range of 3 dB for both methods of defining the sea spike and is listed with 95% confidence levels and correlation coefficients ρ [*Bendat and Piersol*, 1986] in the upper portion of Table 1.

The relative importance of the sea spike contribution to

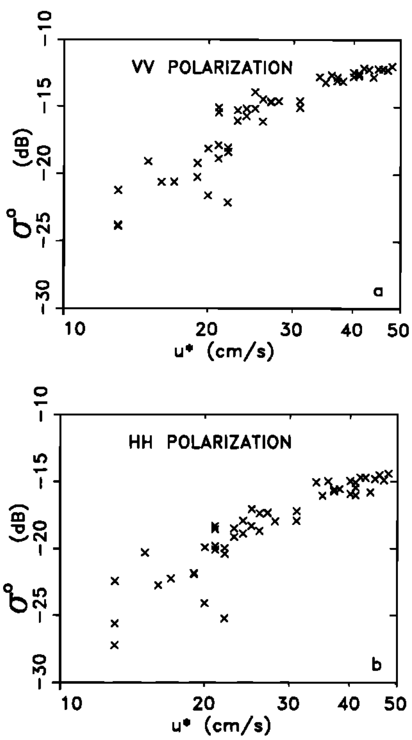

Fig. 6. The normalized radar cross-section versus friction velocity u_*, for (*a*) *VV* and (*b*) *HH* polarization (each point represents a 1-hour record). Note the relatively large amount of scatter for low u_* values compared with the high degree of correlation for large u_*.

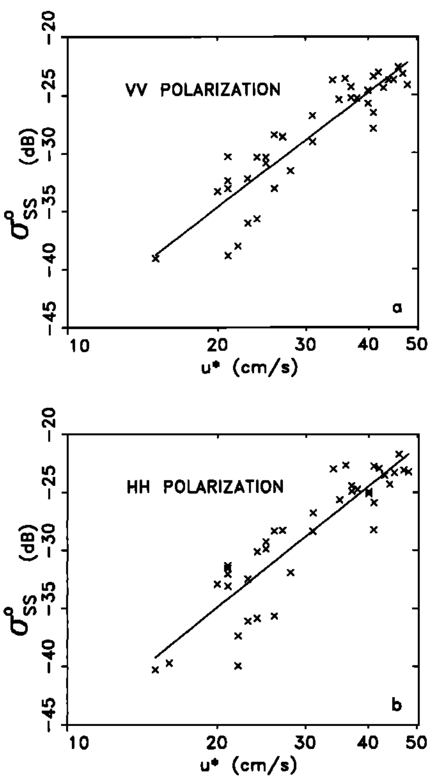

Fig. 7. The sea spike contribution σ^0_{SS} to the normalized radar cross-section versus friction velocity u_* based on method 1 and a threshold of $\bar{\sigma}(t) = -7.2$ dB. The slope of the least squares line is 3.3 for *VV* polarization (Figure 7*a*) and 3.5 for *HH* (Figure 7*b*), indicating a roughly cubic dependence.

the mean radar cross section is of interest for improving current models for σ^0. Figure 8 shows the fractional cross-section due to sea spikes, σ^0_{SS}/σ^0, versus friction velocity for the cross-section threshold of -7.2 dB. Clearly, sea spikes contribute a greater fraction of the return power for *HH* than for *VV* polarization. In general, the average polarization ratio $\sigma^0_{VV}/\sigma^0_{HH}$ is greater than unity [*Wright*, 1966], but during a breaking event the instantaneous polarization ratio can approach or equal unity [*Kwoh and Lake*, 1986]. Therefore the larger contribution of sea spikes to σ^0_{HH} is expected. The value of the fractional radar cross section is of course a function of the cross-section threshold. For the threshold of -7.2 dB, the percentage of the return power due to sea spikes with $25° \le \varphi \le 45°$ at high friction velocity is approximately 5–10% for *VV* polarization and 10–20% for *HH* polarization.

The residual radar cross section, σ^0_{res}, given by

$$\sigma^0_{\text{res}} = \sigma^0 - \sigma^0_{SS} \tag{14}$$

with method 1 for the threshold of -7.2 dB is plotted versus friction velocity in Figure 9. Since the maximum sea spike contribution for this threshold is 20% (approximately 1 dB for *HH* polarization at large u_*), Figure 9 is similar in appearance to the plot of σ^0 in Figure 6. As with Figure 6, the scatter of the data in Figure 9 at lower values of u_* does not suggest a least square fit over the entire range of u_*. The fit for $u_* \ge 23$ cm s^{-1} shown in Figure 9, for which a high degree of correlation is apparent, gives exponents very nearly equal to unity: 1.1 ± 0.2 ($\rho = 0.93$) for *VV* polarization and 1.1 ± 0.2 ($\rho = 0.92$) for *HH* polarization.

Figure 10 shows the frequency of occurrence of sea spikes for the threshold of -7.2 dB as the number of events N in each 1-hour record for which at least two events were counted and the sea spike contribution was at least 1%, that is for $N > 1$ and $\sigma^0_{SS}/\sigma^0 \ge 0.01$. The least squares fit,

$$N = C_2 u_*^{\delta} \tag{15}$$

finds friction velocity exponents of 2.8 for both *VV* and *HH* polarization, for the threshold of -7.2 dB. The exponents δ and correlation coefficients ρ for a threshold range of 3 dB are given in the lower portion of Table 1. As with the friction velocity dependence of σ^0_{SS}, the exponent δ does not significantly change over this threshold range.

The friction velocity exponents computed for both the sea spike contribution to the mean cross section and the frequency of occurrence are all close to 3 (see Table 1). This similar dependence on u_* implies that σ^0_{SS} and N may be linearly related. Therefore in Figure 11 we have plotted N, the number of events in each 1-hour record, against σ^0_{SS} for the threshold of -7.2 dB. The exponents η for

$$N = C_3 \sigma_{SS}^{0\eta} \tag{16}$$

are 0.82 ± 0.06 ($\rho = 0.98$) and 0.77 ± 0.05 ($\rho = 0.98$) for *VV* and *HH* polarization, respectively.

4. DISCUSSION

The argument may be made that sea spikes defined by a rationally chosen yet somewhat arbitrary intensity threshold may not necessarily be due to breaking events. For instance,

TABLE 1. Friction Velocity Exponents

	Threshold, dB		
	−9.0	−7.2	−6.0
	$\sigma_{ss}^0 = C_1 u_*^\alpha$		
Method 1			
VV	3.3 ± 0.5 (0.91)	3.3 ± 0.5 (0.90)	3.2 ± 0.7 (0.85)
HH	3.1 ± 0.5 (0.90)	3.5 ± 0.6 (0.89)	3.4 ± 0.6 (0.89)
Method 2			
VV	3.8 ± 0.5 (0.93)	3.6 ± 0.6 (0.89)	3.6 ± 0.7 (0.88)
HH	3.3 ± 0.5 (0.91)	3.5 ± 0.6 (0.89)	3.5 ± 0.7 (0.88)
	$N = C_2 u_*^\delta$		
VV	3.6 ± 0.6 (0.89)	2.8 ± 0.5 (0.89)	3.0 ± 0.6 (0.88)
HH	3.0 ± 0.6 (0.84)	2.8 ± 0.4 (0.91)	2.7 ± 0.5 (0.87)

Correlation coefficients ρ are given in parentheses.

the random nature of the distribution of scatterers on the sea surface may lead to constructive interference resulting in a sea spike's having little to do with breaking. This argument is diminished by the distributions shown in Figure 3, which indicates that large peak radar cross sections are generally associated with large surface scatter velocities. Furthermore, the choice of a relatively large threshold ensures that the sea spikes counted will be associated with positive surface scatterer velocities.

For friction velocities below 20 cm s^{-1} or so, fewer than 10 events per hour were counted for the chosen threshold of −7.2 dB (see Figure 10). *Melville* [1977] suggested that a minimum friction velocity for the onset of breaking may occur in the neighborhood of 23 cm s^{-1}. Thus deletion of low friction velocity points from Figure 10 and also from Figure 7 might be justified on the grounds that virtually no breaking events occur. However, the minimum friction velocity for the onset of breaking is likely to depend on other factors not available in this data set. For example, long wave slope has been shown to affect σ^0 at X band [*Keller et al.*, 1985], especially at low wind speeds. Indeed, the increased scatter of σ^0 for low u_* in Figure 6 may be an indication of this effect. Removal of the low-velocity data does not significantly change the computed exponents, and thus we present all available data in the interest of completeness.

The residual radar cross section given by (14) and plotted in Figure 9 (as well as the total radar cross-section in Figure 6) shows much less scatter for the larger values of u_*. This observation motivated the linear fit over the higher friction velocity values shown in Figure 9. The residual radar cross-section σ_{res}^0 corresponds to *Phillips'* [1988] Bragg contribution (equation (3)) which is based on the wave spectral density $\psi(\mathbf{k})$ given by (2). The derivation of the spectral density assumes that losses due to breaking are important in the equilibrium range of validity of $\psi(\mathbf{k})$ [*Phillips*, 1985]. Since little wave breaking is expected at low u_*, the friction velocity exponents close to unity for σ_{res}^0 at higher u_* might be interpreted as supporting Phillips' predicted linear dependence. Strictly speaking, however, equation (3) for the Bragg contribution should not be applied to these data (Bragg wavelength of 1.51 cm), since $\psi(\mathbf{k})$ is derived only for gravity waves.

The scatter in the plot of N versus σ_{SS}^0 (Figure 11) is significantly less than that for each quantity plotted individually against u_* (Figures 7 and 10). The nearly linear

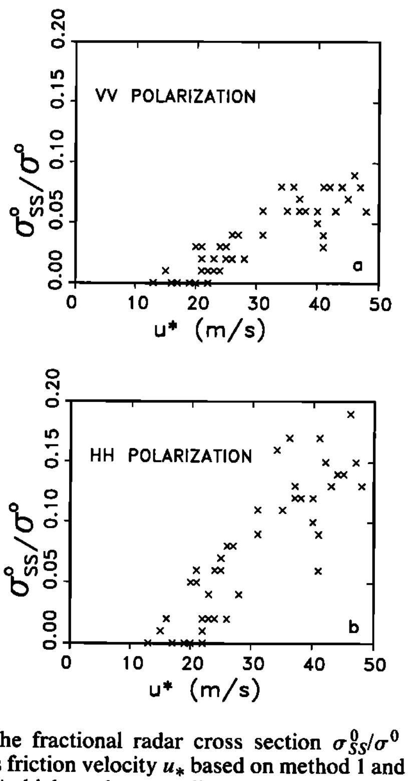

Fig. 8. The fractional radar cross section σ_{SS}^0/σ^0 due to sea spikes versus friction velocity u_* based on method 1 and a threshold of −7.2 dB. At high u_* the sea spike contribution to the mean cross section measured between 25° and 45° relative to the wind is approximately 5–10% for *VV* polarization (Figure 8*a*) and 10–20% for *HH* (Figure 8*b*).

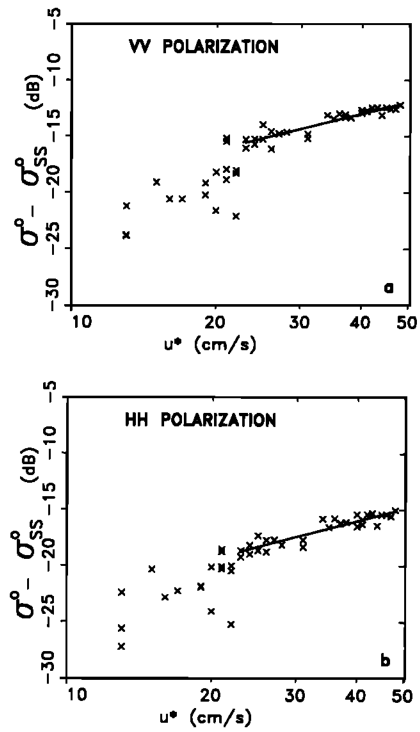

Fig. 9. The residual radar cross section, $\sigma^0 - \sigma_{SS}^0$, versus friction velocity u_* for (*a*) *VV* and (*b*) *HH* polarization. For $u_* \geq 23$ cm s^{-1}, there is very little scatter in the data, and the slope of the least square fit over this range is 1.1 for both polarizations, indicating an approximately linear dependence.

dependence between the sea spike contribution to the radar cross section and the frequency of occurrence of sea spikes implies that the average radar cross section of a sea spike, i.e., σ^0_{SS}/N, may be independent of u_*.

That σ^0_{SS}/N is independent of u_* may be a consequence of the illumination area's being small compared with the dominant surface wavelength. For example, if specular reflection from the steep forward face of a breaking wave is important, then a maximum detectable intensity would be reached when specular scattering occurs over the entire illumination area. Similarly, if the cross section increases with the size of the active breaking region, then a maximum detectable return might occur when the scale of the breaking crest reaches the dimensions of the spot size. In both cases, the cross section measurement would be limited by spot size, and thus above some u_* threshold the average sea spike return might be constant.

On the other hand, an average sea spike cross section which is independent of u_* might be consistent with the fact that breaking occurs over a wide range of scales. If the cross section of a breaking wave is a measure of its size, then the size distribution of breakers and the increase in the number of breaking events at all scales might be such that the average sea spike return is invariant.

5. CONCLUSIONS

Field and laboratory measurements of microwave backscatter at moderate incidence in the presence of wave breaking have indicated that steep and breaking waves produce events referred to as sea spikes. We have presented quantitative measurements of the relationship between the

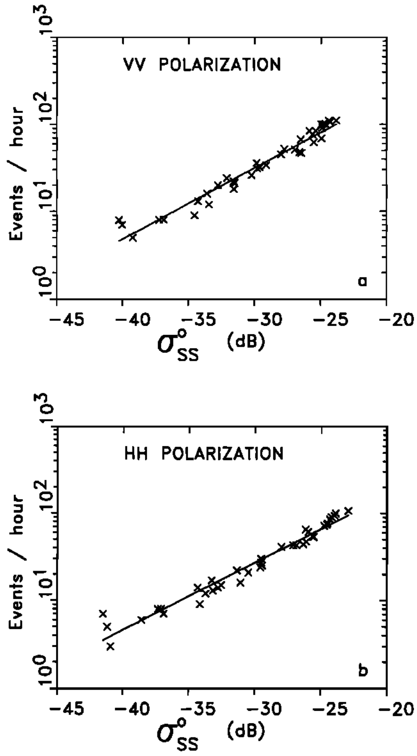

Fig. 11. The frequency of occurrence of sea spikes, N, plotted against sea spike contribution σ^0_{SS} to the normalized radar cross section. The slope of the least squares fit is 0.77 for *VV* polarization (Figure 11*a*) and 0.82 for *HH* (Figure 11*b*). The nearly linear dependence suggests that the cross section of an average sea spike, i.e., σ^0_{SS}/N, may be independent of u_*.

friction velocity u_* and sea spikes for the K_u band radar cross section. The intensity threshold for the definition of the sea spike contribution to the mean radar cross section was chosen to count large sea spikes associated with a positive mean Doppler frequency.

The variation of the sea spike contribution σ^0_{SS} with friction velocity was found to be consistent with *Phillips*' [1988] prediction of a cubic dependence (equation (7)). The fractional power for high friction velocities ($u_* \approx$ 40–50 cm s^{-1}) measured 25° to 45° relative to the wind was found to be approximately 5–10% for *VV* polarization and 10–20% for *HH* polarization with the procedure designated method 1 (equations (10) and (11) and Figure 5*a*). These findings support the inclusion of breaking waves in scattering models for *HH* polarization.

The frequency of occurrence of sea spikes was computed as the number of events counted in a 1-hour record for the chosen threshold. The roughly cubic dependence on friction velocity is consistent with theoretical modeling and field measurements of whitecap coverage reported by other investigators and with *Phillips*' [1988] result (equation (8)). Finally, the data suggest that the contribution of an average sea spike to σ^0 may be independent of u_*.

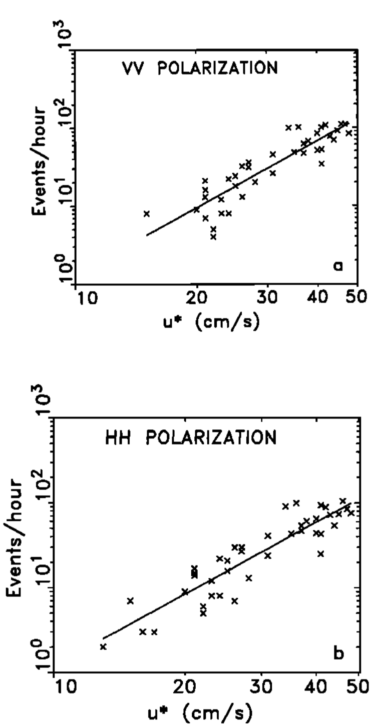

Fig. 10. The frequency of occurrence of sea spikes in terms of number of events in a 1-hour record, N, versus friction velocity u_* for (*a*) *VV* and (*b*) *HH* polarization. The slope of the least squares fit is 3.5 for *VV* and 3.1 for *HH*, indicating an approximately cubic dependence.

Acknowledgments. We gratefully acknowledge the efforts of Finn Hansen of Risø National Laboratory, Roskilde, Denmark, in providing the measurements of friction velocity under ONR contract N00014-87-G-0271. The use of video equipment provided by Peter Lobemier of FWG, Kiel, West Germany was much appreciated. We extend our thanks to the crew of the Forschungsplattform

NORDSEE for their excellent support. We also wish to thank William J. Plant for his helpful comments on an early draft of this paper. One of us (W.K.M.) wishes to thank Tom Spence (formerly of ONR) for his early support and encouragement of this work. The participation of W.K.M. and A.T.J. was supported by grants from the MIT Sloan Basic Research Fund, NSF (Physical Oceanography), and ONR (Physical Oceanography) to W.K.M. The participation of A.T.J. was also supported by the NASA Graduate Student Researchers' Fellowship Program (grant NGT-50292). A preliminary version of these results was first presented at the 1988 Fall meeting of the American Geophysical Union (Jessup et al., 1988).

REFERENCES

Alpers, W., D. B. Ross, and C. L. Rufenach, On the detectability of ocean surface wave by real and synthetic aperture radar, *J. Geophys. Res.*, *86*(C7), 6481–6498, 1981.

Banner, M. L., and E. H. Fooks, On the microwave reflectivity of small-scale breaking water waves, *Proc. R. Soc. London, Ser. A*, *399*, 93–109, 1985.

Bendat, J. S., and A. G. Piersol, *Random data: Analysis and Measurement Procedures*, 2nd ed., Wiley-Interscience, New York, 1986.

Donelan, M., and W. J. Pierson, Jr., Radar scattering and equilibrium ranges in wind-generated wave with application to scatterometry, *J. Geophys. Res.*, *92*(C5), 4971–5092, 1987.

Doviak, R. J., and D. S. Zrnić, *Doppler Radar and Weather Observations*, Academic, San Diego, Calif., 1984.

Duncan, J. R.. W. C. Keller, and J. W. Wright, Fetch and wind speed dependence of Doppler spectra, *Radio Sci.*, *9*, 809–819, 1974.

Ewell, G. W., M. T. Tuley, and W. F. Horne, Temporal and spatial behavior of high resolution sea clutter 'spikes,' *IEEE Radar '84 Conf.*, 100–104, 1984.

Guinard, N. W., J. T. Ransome, and J. C. Daley, Variation of the NRCS of the sea with increasing roughness, *J. Geophys. Res.*, *76*, 1525–1538, 1971.

Holthuijsen, L. H., and T. H. C. Herbers, Statistics of breaking waves observed as whitecaps in the open sea, *J. Phys. Oceanogr.*, *16*, 290–297, 1986.

Jessup, A. T., Microwave detection and characterization of deep-water wave breaking, M.S. thesis, Mass. Inst. of Technol. Cambridge, Mass., May 1988.

Jessup, A. T., Detection and characterization of deep water wave breaking using moderate incidence angle microwave backscatter from the sea surface, Ph.D. thesis, 360 pp., Joint Program in Oceanogr. and Oceanogr. Eng., Mass. Inst. of Technol./Woods Hole Oceanogr. Inst., Woods Hole, Mass., 1990.

Jessup, A. T., W. C. Keller, W. K. Melville, Microwave detection and characterization of deep-water wave breaking (abstract), *Eos Trans. AGU*, *69*(44), 1245, 1988.

Kalmykov, A. I., and V. V. Pustovoytenko, On the polarization features of radio signal scattered from the sea surface at small grazing angles, *J. Geophys. Res.*, *81*, 1960–1964, 1976.

Katzin, M., On the mechanism of radar sea clutter, *Proc. IRE*, *45*, 44–54, 1957.

Keller, W. C., W. J. Plant, and D. E. Weissman, The dependence of *X* band microwave sea return on atmospheric stability and sea state, *J. Geophys. Res.*, *90*(C1), 1019–1029, 1985.

Keller, W. C., W. J. Plant, and G. R. Valenzuela, Observations of breaking ocean waves with coherent microwave radar, in *Wave Dynamics and Radio Probing of the Sea Surface*, edited by O. M. Phillips and K. Hasselmann, Plenum, New York, 1986.

Keller, W. C., V. Wismann, and W. Alpers, Tower-based measurements of the ocean *C* band radar backscattering cross section, *J. Geophys. Res.*, *94*(C1), 924–930, 1989.

Kwoh, D. S. W., and B. M. Lake, A deterministic, coherent, and dual-polarized laboratory study of microwave backscattering from water waves, 1, Short gravity waves without wind, *IEEE J. Oceanic Eng.*, *OE-9*, 291–308, 1984.

Kwoh, D. S., and B. M. Lake, Microwave backscatter from short gravity waves: deterministic, coherent, dual-polarized study of the relationship between backscatter and water wave properties, in *Wave Dynamics and Radio Probing of the Sea Surface*, edited by O. M. Phillips and K. Hasselmann, pp. 443–447, Plenum, New York, 1986.

Kwoh, D. S., B. M. Lake, and H. Rungaldier, Microwave scattering from internal wave modulated surface waves: A shipboard real aperture coherent radar study in the Georgia Strait Experiment, *J. Geophys. Res.*, *93*(C10), 12,235–12,248, 1988.

Lewis, B. L., and I. D. Olin, Experimental study and theoretical model of high-resolution radar backscatter from the sea, *Radio Sci.*, *15*, 815–828, 1980.

Long, M. W., On the two-scatterer theory of sea echo, *IEEE Trans. Antennas Propag.*, *AP-22*, 667–672, 1974.

Long, M. W., *Radar Reflectivity of Land and Sea*, pp. 502–505, Artech House, Dedham, Mass., 1983.

Lyzenga, D. R., A. L. Maffett, and R. A. Shuchman, The contribution of wedge scattering to the radar cross-section of the ocean surface, *IEEE Trans. Geosci. Remote Sens.*, *GE-21*(*4*), 1983.

Melville, W. K., Wind stress and roughness length over breaking waves, *J. Phys. Oceanogr.*, *7*, 702–710, 1977.

Melville, W. K., M. R. Loewen, F. C. Felizardo, A. T. Jessup, and M. J. Buckingham, Acoustic and microwave signatures of breaking waves, *Nature*, *336*(6194), 54–59, 1988.

Monahan, E. C., and I. G. O'Muircheartaigh, Whitecaps and the passive remote sensing of the ocean surface, *Int. J. Remote Sens.*, *7*(5), 627–642, 1986.

Phillips, O. M., Spectral and statistical properties of the equilibrium range in wind-generated gravity waves, *J. Fluid Mech.*, *156*, 505–531, 1985.

Phillips, O. M., Radar returns from the sea surface—Bragg scattering and breaking waves, *J. Phys. Oceanogr.*, *18*, 1065–1074, 1988.

Phillips, O. M., and M. L. Banner, Wave breaking in the presence of wind drift and swell, *J. Fluid Mech.*, *66*, 625–640, 1974.

Plant, W. J., and W. C. Keller, The two-scale radar wave probe and SAR imagery of the ocean, *J. Geophys. Res.*, *88*(C14), 9776–9784, 1983.

Ross, D. B., and V. Cardone, Observations of oceanic whitecaps and their relation to remote measurements of surface wind speed, *J. Geophys. Res.*, *79*(3), 444–452, 1974.

Wright, J. W., Backscattering from capillary waves with application to sea clutter, *IEEE Trans. Antennas Propag.*, *AP-14*, 749–754, 1966.

Wu, J., Oceanic whitecaps and sea state, *J. Phys. Oceanogr.*, *9*, 1064–1068, 1979.

Wu, J., Wind-stress coefficients over sea surface near neutral conditions—A revisit, *J. Phys. Oceanogr.*, *10*, 727–740, 1980.

A. T. Jessup and W. K. Melville, Massachusetts Institute of Technology, Cambridge, MA 02139.

W. C. Keller, U.S. Naval Research Laboratory, Code 8310-140, Washington, DC 20375.

(Received April 19, 1989;
accepted August 31, 1989.)